

Precise Control of Pi-electron Magnetism in Metal-free Porphyrins

Yan Zhao, Kaiyue Jiang, Can Li, Yufeng Liu, Chengyang Xu, Wenna Zheng, Dandan Guan, Yaoyi Li, Hao Zheng, Canhua Liu, Weidong Luo, Jinfeng Jia, Xiaodong Zhuang, and Shiyong Wang

J. Am. Chem. Soc., **Just Accepted Manuscript** • DOI: 10.1021/jacs.0c07791 • Publication Date (Web): 22 Sep 2020

Downloaded from pubs.acs.org on September 22, 2020

Just Accepted

“Just Accepted” manuscripts have been peer-reviewed and accepted for publication. They are posted online prior to technical editing, formatting for publication and author proofing. The American Chemical Society provides “Just Accepted” as a service to the research community to expedite the dissemination of scientific material as soon as possible after acceptance. “Just Accepted” manuscripts appear in full in PDF format accompanied by an HTML abstract. “Just Accepted” manuscripts have been fully peer reviewed, but should not be considered the official version of record. They are citable by the Digital Object Identifier (DOI®). “Just Accepted” is an optional service offered to authors. Therefore, the “Just Accepted” Web site may not include all articles that will be published in the journal. After a manuscript is technically edited and formatted, it will be removed from the “Just Accepted” Web site and published as an ASAP article. Note that technical editing may introduce minor changes to the manuscript text and/or graphics which could affect content, and all legal disclaimers and ethical guidelines that apply to the journal pertain. ACS cannot be held responsible for errors or consequences arising from the use of information contained in these “Just Accepted” manuscripts.

Precise Control of π -electron Magnetism in Metal-free Porphyrins

Yan Zhao^{1†}, Kaiyue Jiang^{2†}, Can Li¹, Yufeng Liu¹, Chengyang Xu¹, Wenna Zheng¹, Dandan Guan^{1,3,4}, Yaoyi Li^{1,3,4}, Hao Zheng^{1,3,4}, Canhua Liu^{1,3,4}, Weidong Luo^{1,5}, Jinfeng Jia^{1,3,4}, Xiaodong Zhuang^{2*}, Shiyong Wang^{1,3,4*}

¹Key Laboratory of Artificial Structures and Quantum Control (Ministry of Education), Shenyang National Laboratory for Materials Science, School of Physics and Astronomy, Shanghai Jiao Tong University, Shanghai 200240, China

²The meso-Entropy Matter Lab, School of Chemistry and Chemical Engineering, Shanghai Jiao Tong University, Shanghai 200240, China

³Tsung-Dao Lee Institute, Shanghai Jiao Tong University, Shanghai, 200240, China.

⁴Shanghai Research Center for Quantum Sciences, Shanghai 201315, China

⁵Institute of Natural Sciences, Shanghai Jiao Tong University, Shanghai, 200240, China.

[†]These authors contributed equally to this work.

*Corresponding Authors: shiyong.wang@sjtu.edu.cn, zhuang@sjtu.edu.cn

ABSTRACT

The porphyrin macrocycle can stabilize a set of magnetic metal ions, thus introducing localized net spins near the center. However, it remains elusive but most desirable to introduce delocalized spins in porphyrins with wide implications, for example, for building correlated quantum spins. Here, we demonstrate that metal-free porphyrins host delocalized π -electron magnetism as revealed by scanning probe microscopy and different level of theory calculations. Our results demonstrate that engineering of π -electron topologies introduces spin polarized singlet state and delocalized net spins in metal-free porphyrins. In addition, the π -electron magnetism can be switched on/off via STM manipulation by tuning the interfacial charge transfer. Our results provide an effective way to precisely control the π -electron magnetism in metal-free porphyrins, which can be further extended to design new magnetic functionalities of porphyrin-based architectures.

INTRODUCTION

1
2
3
4
5 Porphyrin molecules have a wide spectrum of physicochemical and biological properties with diverse applications
6
7 in sensors, molecular electronics/spintronics and medical applications¹⁻³. The rich functionalities of porphyrin
8
9 complexes originate from the center macrocycle, which can stabilize a variety of elements inside and thus gives
10
11 rise to distinct structural, electronic, magnetic, optoelectronic, and transport properties⁴⁻¹³. Magnetic
12
13 metalloporphyrins have been extensively studied by various techniques, exhibiting kondo and spin excitation
14
15 effects, Yu-Shiba bound states, and spin-state switching¹³⁻²⁷. Recently, hybridized graphene and metalloporphyrin
16
17 nanostructures have been achieved, hosting combined intriguing electronic and magnetic properties²⁸⁻³³. The
18
19 magnetism of metalloporphyrin architectures originates from the stabilized metal ions, and thus localizes at the
20
21 center of the molecules. It remains elusive but most desirable to develop strategies to introduce delocalized spins
22
23 in porphyrins for designer new magnetic functionalities in porphyrin architectures.

24
25 Recent advances of on-surface synthesis allow for tailoring π -electron topologies at the single chemical bond level,
26
27 and thus provide the ability to precisely engineer π -electron magnetism in low-dimensional graphene
28
29 nanostructures by introducing sublattice imbalance, topological frustration and topological defects³⁴⁻⁵⁰. Examples
30
31 like triangulenes^{41,43,48,51}, bowtie-shape nanographenes⁴⁷, chiral graphene nanoribbons⁴⁵, polymers⁵² and
32
33 nanographenes with topological defects^{46,49} have been recently synthesized and characterized on surfaces. Similar
34
35 as nanographenes, the porphyrin macrocycle is aromatic and can be interpreted as a multiple-bridged aromatic
36
37 diaza[18]annulene system^{53,54}. Thorough tailoring peripheral π -electron topology, it is in principle able to
38
39 introduce tunable π -electron magnetism in metal-free porphyrin architectures, thus greatly enriching magnetic
40
41 functionalities of porphyrin-based systems. Although substituted open-shell porphyrins have been realized using
42
43 conventional solution synthesis methods, on-surface synthesis of unsubstituted porphyrins with π -electron
44
45 magnetism remains to be explored^{55,56}.

46
47 Here, we demonstrate such ability to precisely control delocalized magnetism in metal-free porphyrins through
48
49 tailoring their peripheral π -electron topologies. Using combined solution and on-surface synthesis, three metal-
50
51 free porphyrins with different π -electron topologies have been synthesized. Their chemical structures have been
52
53 resolved by using high resolution non-contact atomic force microscopy, permitting us to clearly distinguish their
54
55 π -electron topologies at the single chemical bond level. Using low-temperature scanning tunneling spectroscopy,
56
57 their π -electron magnetism has been confirmed by Kondo effects. The experimental observations can be nicely
58
59 elucidated by clear empirical rule, mean-field Hubbard model and spin-polarized density functional theory
60
calculations. In addition, the π -electron magnetism can be reversibly switched on/off via STM manipulation by

1
2
3 tuning the charge transfer from the underneath metal substrate. The realization of π -electron magnetism in metal-
4 free porphyrin may be further extended to build correlated spins in porphyrin-based nanostructures, with
5 implications for quantum information and spintronics applications.
6
7
8
9

10 RESULTS AND DISCUSSION

11 Using combined in-solution and on-surface synthesis, metal-free porphyrins with different π -electron topologies
12 have been synthesized. As shown in Fig. 1a, the precursor 5,10,15,20-tetrakis(2,6-dimethylphenyl)porphyrin is
13 synthesized in solution by using freshly distilled pyrrole and 2,6-dimethylbenzaldehyde (cf. detailed synthesis
14 method in supplementary fig. 1). After in-solution synthesis, the precursor is thermally deposited on a Au(111)
15 substrate held at room temperature following a subsequent annealing to 295 °C for 10 minutes. At elevated
16 temperature, thermal-induced cyclodehydrogenation of methyl units occurs, giving rise to fully aromatic
17 porphyrins^{39,57}. Except for the main cyclodehydrogenation, two common side reactions take place occasionally on
18 Au(111): i) few methyl units detach from the precursors forming five-membered carbon rings after subsequent
19 cyclodehydrogenation, and ii) partial dehydrogenation of methyl unit (or post passivation of radical carbon sites
20 by additional hydrogens) sometimes occurs and introduces sp^3 hybridized carbon sites at edges. As shown in Fig.
21 1b, three products have been frequently observed and characterized. The Product #1 contains two pentagon carbon-
22 rings at opposite sides, and the Product #3 has a sp^3 hybridized carbon site passivated by two hydrogen atoms. In
23 addition, we also observed some molecules are metalated by Au adatoms, forming Au-Porphyrin complexes. Their
24 chemical structures have been clearly resolved by high resolution nc-AFM imaging using a CO-functionalized tip
25 (cf. Fig. 1c-e). The number of unpaired π -electrons (radicals) in the resulted porphyrins has been determined by
26 using Clar's empirical rule (cf. all the possible π -electron networks in supplementary Fig. 4 and 5)^{58,59}. As shown
27 in Fig. 1, the Product #1 is a closed-shell molecule, while the Product #2 and #3 have two and one unpaired π -
28 electron(s), respectively (as marked by red dots in Fig. 1). The presence of radicals suggests an open-shell
29 configuration in the Product #2 and #3, thus giving rise to delocalized π -electron magnetism.
30
31
32
33
34
35
36
37
38
39
40
41
42
43
44
45
46
47
48
49

50 The energy spectra and frontier molecular orbitals of the resulted porphyrins have been calculated by using mean-
51 field Hubbard model (MFHM) and spin- polarized density functional theory (SP-DFT), which have been widely
52 used to determine the magnetic structure of nanographenes and show nice agreements with experiments³⁷. As
53 shown in Fig. 2a-c, the Product #1 has a closed-shell ground state as confirmed by combined Clar empirical rule,
54 MFHM and SP-DFT calculations. Experimentally, differential conductance (dI/dV) spectroscopy has been used
55 to detect the electronic structure of achieved porphyrins. High resolution dI/dV mappings are able to resolve spatial
56 distribution of molecular orbitals. As shown in Fig. 2d, dI/dV spectra taken above the center of the Product #1
57
58
59
60

1
2
3 reveal two resonances at -1.4 V and 0.9 V, which can be assigned to the highest occupied molecular orbital (HOMO)
4 and lowest unoccupied molecular orbital (LUMO), respectively. dI/dV mappings at these two energies resolve the
5 spatial distribution of these two molecular states, which agree well with HOMO and LUMO orbital shapes as
6 calculated by MFHM and SP-DFT. In addition, we did not observe the kondo resonance near the fermi level. These
7 results confirm that the Product #1 is a closed-shell molecule without any unpaired π -electrons.
8
9
10

11
12
13 Despite its slightly different π -electron topology from that of the Product #1, the Product #2 has drastically
14 different magnetic ground state. The Product #2 has in total 58 π - electrons, with 2 π -electrons more than those of
15 the Product #1. Although both of them host even number of π -electrons, the Product #2 has an open-shell electronic
16 structure as opposed to the closed-shell configuration of the Product #1 (cf. Fig. 3a). The reason is due to
17 topological frustration, that is, it is impossible to concomitantly pair all p_z orbitals to form π bonds in the Product
18 #2. This picture can be verified by both MFHM and SP-DFT calculations as shown in figure 3b-e. The calculated
19 energy levels in Fig. 3b-c show that there are two degenerated states below fermi level, which are spatially
20 separated with enhanced orbital density at opposite sides (cf. Fig. 3d and e), and singly occupied by two electrons
21 with oppositely oriented spins. In other words, the ground electronic configuration breaks spin-spatial symmetry
22 and exhibits antiferromagnetic ordering, which can be nicely seen in the calculated spin density maps in Fig. 3f
23 and g. The mechanism behind is very similar to Clar Goblet, where topological frustration induces spin polarized
24 singlet state in the bowtie-shape nanographene^{36,47}.
25
26
27
28
29
30
31
32
33
34
35
36
37

38 However, experimental dI/dV measurements reveal that the Product #2 hosts a net spin of $S=1/2$ by showing a
39 sharp Kondo resonance instead of the expected singlet ground state with a net spin of $S=0$ (cf. Fig. 4g). As
40 illustrated in Fig. 4a, we attribute this discrepancy to the interfacial charge transfer, where one electron is
41 transferred from molecule to gold substrate making it positively charged. We can exclude the possibility of
42 negative charging through comparing spin density distributions differences (cf. supplementary Fig. 11). Similar
43 charging effects have been previously observed in several graphene nanostructures, such as the zigzag termini of
44 $N=7$ armchair graphene nanoribbons^{60,61}, and $N=6$ zigzag graphene nanoribbon³⁹ (N denotes the width of graphene
45 nanoribbons in terms of the number of carbon atoms). As shown in Fig. 4b-c, the electronic structure of the
46 positively charged Product #2 is calculated by MFHM and SP-DFT, revealing a singly occupied molecular state
47 below fermi level. This means the charged molecule is with a net magnetic moment of $S=1/2$. On metal substrate,
48 this magnetic moment will be screened by Au(111) electron reservoir, which can be understood by single impurity
49 Anderson Model^{17,62}. As shown in Fig. 4g, dI/dV spectra reveal such screening effect by showing a sharp Kondo
50 resonance at Fermi level. In addition, the observed spin density distribution nicely agrees with calculated results,
51
52
53
54
55
56
57
58
59
60

1
2
3 further supporting that the observed zero-bias peak originates from Kondo resonance (cf. Fig. 4d-f). As per
4 Anderson model, the Kondo peak width varies with temperature with full width at half maximum (FWHM) of $\Gamma =$
5 $\sqrt{(\alpha k_B T)^2 + (2k_B T_K)^2}$, where T is the temperature, T_K is the Kondo temperature, and α is the slope of linear
6
7 growth of the width at $T \gg T_K$. The experimental obtained temperature dependent FWHM can be well fitted by
8
9 the previous equation, giving a Kondo temperature of 22 K (cf. Fig 4h-i and supplementary Fig.6). We can exclude
10
11 that the sharp Kondo resonance originates from a high-spin state of S=1 by measuring its response to magnetic
12
13 field (cf. supplementary Fig. 7).
14
15

16
17 Using similar techniques, the magnetic properties of the Product #3 has been determined. Since one carbon site is
18
19 passivated by two hydrogen atoms, the Product #3 has one π -electron less than the Product #2 with an odd number
20
21 of 57 π -electrons in total. It is impossible to concomitantly pair odd number of p_z orbitals to form π bonds, thus
22
23 generating one π radical as marked by a red dot in Fig. 5a. MFHM and SP-DFT calculations confirm the presence
24
25 of a singly occupied state below fermi level in the Product #2, that is, a net spin of S=1/2. As shown in Fig. 5d, the
26
27 passivation of π -radical locally modifies its spin density distribution, which gets significantly quenched near the
28
29 CH_2 site (cf. Clar non-kekulé structures in Supplementary Fig. 4). The emergence of net spins in porphyrins with
30
31 odd number of π electrons is very similar to nanographenes with sublattice imbalance as proposed by E. Lieb in
32
33 1989³⁴. As shown in Fig. 5g, dI/dV spectroscopy measurements confirm the emergence of a net spin of S=1/2 in
34
35 the Product #3. The net spin couples with underneath electron reservoir, generating Kondo resonances by showing
36
37 a sharp Fano-shape peak at fermi level in dI/dV spectra with peak intensity proportional to spin density magnitude.
38
39 In addition, the resolved spin density distribution fits very well with the calculated result (cf. Fig. 5e and f). The
40
41 nice agreements between experiments and calculations in gas phase indicate that the Product #3 is neutral on
42
43 Au(111).
44
45

46 Although the Product #3 shares very similar adsorption geometries with that of the Product #2, the former is neutral
47
48 on Au(111) while the latter is positively charged. By carefully checking the AFM images in Fig. 1c-e, one can see
49
50 that the presence of sp^3 carbon (CH_2) site slightly lifts the corner near the CH_2 site away from the surface, which is
51
52 imaged as a local bright protrusion in nc-AFM imaging due to a stronger Pauli repulsion. This slight adsorption
53
54 difference leads to a completely different charging behavior. Previous DFT calculations by using a set of van der
55
56 Waals correction schemes reveal that despite very similar adsorption heights of most graphene nanostructures on
57
58 Au(111), the magnetism (charge transfer) is very sensitive to small perturbations (adsorption height variations),
59
60 supporting our observations⁶³. To gain more evidences of the charging effect, we performed STM manipulation to
locally modify the adsorption configurations. After each manipulation, we performed nc-AFM imaging, constant-

1
2
3 height current imaging and dI/dV spectroscopy to trace the charging transfer. As shown in fig. 6a, the porphyrin
4 molecule is initially neutral by showing a Kondo resonance at Fermi level. After manipulation, the molecule rotates
5 an angle of 185° around the out-of-plane axis (cf. Fig. 6b). Although nc-AFM and constant-height current image
6 indicate a similar adsorption geometry after rotation, dI/dV spectroscopy reveals that the molecule is positively
7 charged by showing a broad peak above Fermi level instead of exhibiting a sharp Kondo resonance at Fermi level
8 (cf. the No. 2 spectrum in Fig. 6d). In other words, the electron previously occupied the singly occupied state
9 transfers to gold substrate, thus making the molecule positively charged and leading all orbitals doubly occupied.
10 Further manipulation experiment was used to rotate the molecule again. As shown in Fig. 6c, the Kondo resonance
11 appears after a successive rotation of 125° , suggesting the molecule becomes neutral again. In total, we performed
12 successive 9 times STM manipulations, and found that the charging effect is extremely sensitive to adsorption
13 variations (cf. supplementary Fig. 10). Similar manipulation experiments have been performed on the Product #1
14 and #2 without obtaining this switching effect. These results indicate that slightly decoupling the molecule from
15 surface can effectively quench the charging effect, such as by lifting the molecule slightly away from the substrate
16 by functional groups. Other possibilities may also change the coupling between molecule and substrate, such as
17 different adsorption sites, Au(111) surface reconstruction (with dangling bond at herringbone corners), etc.

18
19
20
21
22
23
24
25
26
27
28
29
30
31
32
33 We notice that the Kondo peak positions slightly shift away from Fermi level. Even for the same molecule, the
34 Kondo peak position as well as peak width varies a little after STM manipulations (cf. Supplementary Fig. 10). As
35 revealed by previous second-order perturbative model, the Kondo shape and peak position depend sensitively on
36 hybridization with substrate as well as charge transfer from substrate¹⁸. Charge transfer from substrate will affect
37 the occupation number, and hence shift the peak center away from Fermi level. Hybridization with substrate will
38 change the peak shape. For the strong hybridization case, the Kondo resonance exhibits a dip in dI/dV spectroscopy.
39 For the case without hybridization, the Kondo resonance behaves as a symmetric peak centered at Fermi level. In
40 our case, the peak shape is slightly asymmetric and centered a little away from Fermi level, indicating a weak
41 hybridization with substrate.
42
43
44
45
46
47
48
49

50 CONCLUSION

51
52
53 In conclusion, we demonstrate an effective approach to engineer π -electron magnetism in metal-free porphyrins
54 by using combined non-contact atomic force microscopy, scanning tunneling microscopy/spectroscopy as well as
55 theory calculations at different levels. Three types of porphyrins with different π -electron topologies have been
56 successively synthesized and characterized down to the single chemical bond level. The π -electron network in
57 porphyrins with even number of π -electron can either host a spin polarized singlet ground state or closed-shell
58
59
60

1
2
3 configuration depending whether the network gets frustrated or not. Porphyrins with odd number of π electrons
4
5 host nets spin similar as sublattice imbalance induced spins in nanographenes. In addition, the magnetism can be
6
7 switched on/off by tuning charge transfer from underneath Au(111). Our method reported herein provides ample
8
9 opportunities for further designer correlated spins in porphyrin-based nanostructures to study their many-body
10
11 effects.

12 13 ASSOCIATED CONTENT

14
15
16 **Supporting Information.** Detailed descriptions of experimental and theoretical procedures, Clar non-kekulé
17
18 structures of the Product #2 and 3, Magnetic field and temperature dependence of Kondo resonance, dI/dV spectra
19
20 and mappings, and simulated local density of state maps. This material is available free of charge via the Internet
21
22 at <http://pubs.acs.org>.

23 24 25 AUTHOR INFORMATION

26
27 Yan Zhao and Kaiyue Jiang contributed equally to this work.

28 29 30 ACKNOWLEDGEMENT

31
32
33 S. W. acknowledges the financial support from the National Natural Science Foundation of China (No. 11874258),
34
35 the Shanghai Municipal Science and Technology Qi Ming Xing Project (No. 20QA1405100) and Fok Ying Tung
36
37 Foundation for young researchers. This work is also supported by the Ministry of Science and Technology of
38
39 China (Grants No. 2016YFA0301003, No. 2016YFA0300403), the National Natural Science Foundation of China
40
41 (Grants No. 11521404, No. 11634009, No. 11574202, No. 11874256, No. 11790313, No. 11674226, No.
42
43 U1632102, No. 11674222, No. U1632272 and No. 11861161003), the Strategic Priority Research Program of
44
45 Chinese Academy of Sciences (Grant No. XDB28000000), and the Shanghai Municipal Science and Technology
46
47 Major Project (Grant No.2019SHZDZX01). Y.L. thanks ECNU Multifunctional Platform for Innovation (001) of
48
49 East China Normal University for providing computing resources.
50
51
52
53
54
55
56
57
58
59
60

REFERENCES

- (1) Kadish, K.; Smith, K.; Guillard, R. *Handbook of Porphyrin Science*; World Scientific Publishing Company, 2010.
- (2) Senge, M. O.; Fazekas, M.; Notaras, E. G. A.; Blau, W. J.; Zawadzka, M.; Locos, O. B.; Ni Mhuircheartaigh, E. M. Nonlinear Optical Properties of Porphyrins. *Adv. Mater.* **2007**, *19* (19), 2737–2774.
- (3) Huang, H.; Song, W.; Rieffel, J.; Lovell, J. F. Emerging Applications of Porphyrins in Photomedicine. *Front. Phys.* **2015**, *3*, 23.
- (4) Baklanov, A.; Garnica, M.; Robert, A.; Bocquet, M.-L.; Seufert, K.; Kuchle, J. T.; Ryan, P. T. P.; Haag, F.; Kakavandi, R.; Allegretti, F.; Auwärter, W. On-Surface Synthesis of Nonmetal Porphyrins. *J. Am. Chem. Soc.* **2020**, *142* (4), 1871–1881.
- (5) Auwärter, W.; Écija, D.; Klappenberger, F.; Barth, J. V. Porphyrins at Interfaces. *Nat. Chem.* **2015**, *7* (2), 105–120.
- (6) Grill, L.; Dyer, M.; Lafferentz, L.; Persson, M.; Peters, M. V.; Hecht, S. Nano-Architectures by Covalent Assembly of Molecular Building Blocks. *Nat. Nanotechnol.* **2007**, *2* (11), 687–691.
- (7) Gottfried, J. M.; Flechtner, K.; Kretschmann, A.; Lukasczyk, T.; Steinrück, H.-P. Direct Synthesis of a Metalloporphyrin Complex on a Surface. *J. Am. Chem. Soc.* **2006**, *128* (17), 5644–5645.
- (8) Zhang, Y.; Luo, Y.; Zhang, Y.; Yu, Y.-J.; Kuang, Y.-M.; Zhang, L.; Meng, Q.-S.; Luo, Y.; Yang, J.-L.; Dong, Z.-C.; Hou, J. G. Visualizing Coherent Intermolecular Dipole–Dipole Coupling in Real Space. *Nature* **2016**, *531* (7596), 623–627.
- (9) Kumagai, T.; Hanke, F.; Gawinkowski, S.; Sharp, J.; Kotsis, K.; Waluk, J.; Persson, M.; Grill, L. Controlling Intramolecular Hydrogen Transfer in a Porphycene Molecule with Single Atoms or Molecules Located Nearby. *Nat. Chem.* **2014**, *6* (1), 41–46.
- (10) Zhao, A.; Li, Q.; Chen, L.; Xiang, H.; Wang, W.; Pan, S.; Wang, B.; Xiao, X.; Yang, J.; Hou, J. G.; Zhu, Q. Controlling the Kondo Effect of an Adsorbed Magnetic Ion Through Its Chemical Bonding. *Science* **2005**, *309* (5740), 1542–1544.
- (11) Chen, X.; Fu, Y.-S.; Ji, S.-H.; Zhang, T.; Cheng, P.; Ma, X.-C.; Zou, X.-L.; Duan, W.-H.; Jia, J.-F.; Xue, Q.-K. Probing Superexchange Interaction in Molecular Magnets by Spin-Flip Spectroscopy and Microscopy. *Phys. Rev. Lett.* **2008**, *101* (19), 197208.
- (12) Kuang, G.; Chen, S.-Z.; Wang, W.; Lin, T.; Chen, K.; Shang, X.; Liu, P. N.; Lin, N. Resonant Charge Transport in Conjugated Molecular Wires beyond 10 Nm Range. *J. Am. Chem. Soc.* **2016**, *138* (35), 11140–11143.
- (13) Köbke, A.; Gutzeit, F.; Röhricht, F.; Schlimm, A.; Grunwald, J.; Tuczek, F.; Studniarek, M.; Longo, D.; Choueikani, F.; Otero, E.; Ohresser, P.; Rohlf, S.; Johannsen, S.; Diekmann, F.; Rosnagel, K.; Weismann, A.; Jasper-Toennies, T.; Näther, C.; Herges, R.; Berndt, R.; Gruber, M. Reversible Coordination-Induced Spin-State Switching in Complexes on Metal Surfaces. *Nat. Nanotechnol.* **2020**, *15* (1), 18–21.
- (14) Girovsky, J.; Nowakowski, J.; Ali, Md. E.; Baljovic, M.; Rossmann, H. R.; Nijs, T.; Aeby, E. A.; Nowakowska, S.; Siewert, D.; Srivastava, G.; Wäckerlin, C.; Dreiser, J.; Decurtins, S.; Liu, S.-X.; Oppeneer, P. M.; Jung, T. A.; Ballav, N. Long-Range Ferrimagnetic Order in a Two-Dimensional Supramolecular Kondo Lattice. *Nat. Commun.* **2017**, *8* (1), 15388.
- (15) Wang, W.; Pang, R.; Kuang, G.; Shi, X.; Shang, X.; Liu, P. N.; Lin, N. Intramolecularly Resolved Kondo Resonance of High-Spin Fe-Porphyrin Adsorbed on Au(111). *Phys. Rev. B* **2015**, *91* (4), 045440.
- (16) Kezilebieke, S.; Žitko, R.; Dvorak, M.; Ojanen, T.; Liljeroth, P. Observation of Coexistence of Yu-Shiba-Rusinov States and Spin-Flip Excitations. *Nano Lett.* **2019**, *19* (7), 4614–4619.
- (17) Ternes, M.; Heinrich, A. J.; Schneider, W.-D. Spectroscopic Manifestations of the Kondo Effect on Single Adatoms. *J. Phys. Condens. Matter* **2009**, *21* (5), 053001.
- (18) Ternes, M. Spin Excitations and Correlations in Scanning Tunneling Spectroscopy. *New J. Phys.* **2015**, *17* (6), 063016.
- (19) Choi, D.-J.; Lorente, N.; Wiebe, J.; von Bergmann, K.; Otte, A. F.; Heinrich, A. J. Colloquium: Atomic Spin Chains on Surfaces. *Rev. Mod. Phys.* **2019**, *91* (4), 041001.
- (20) Li, X.; Zhu, L.; Li, B.; Li, J.; Gao, P.; Yang, L.; Zhao, A.; Luo, Y.; Hou, J.; Zheng, X.; Wang, B.; Yang, J. Molecular Molds for Regularizing Kondo States at Atom/Metal Interfaces. *Nat. Commun.* **2020**, *11* (1), 2566.

- 1
2
3 (21) Liu, L.; Yang, K.; Jiang, Y.; Song, B.; Xiao, W.; Li, L.; Zhou, H.; Wang, Y.; Du, S.; Ouyang, M.; Hofer, W. A.; Castro Neto, A. H.; Gao, H.-J. Reversible Single Spin Control of Individual Magnetic Molecule by Hydrogen Atom Adsorption. *Sci. Rep.* **2013**, *3* (1), 1210.
- 4
5
6 (22) Zhang, Q.; Kuang, G.; Pang, R.; Shi, X.; Lin, N. Switching Molecular Kondo Effect via Supramolecular Interaction. *ACS Nano* **2015**, *9* (12), 12521–12528.
- 7
8 (23) Iancu, V.; Deshpande, A.; Hla, S.-W. Manipulating Kondo Temperature via Single Molecule Switching. *Nano Lett.* **2006**, *6* (4), 820–823.
- 9
10 (24) Flechtner, K.; Kretschmann, A.; Steinrück, H.-P.; Gottfried, J. M. NO-Induced Reversible Switching of the Electronic Interaction between a Porphyrin-Coordinated Cobalt Ion and a Silver Surface. *J. Am. Chem. Soc.* **2007**, *129* (40), 12110–12111.
- 11
12 (25) Tsukahara, N.; Shiraki, S.; Itou, S.; Ohta, N.; Takagi, N.; Kawai, M. Evolution of Kondo Resonance from a Single Impurity Molecule to the Two-Dimensional Lattice. *Phys. Rev. Lett.* **2011**, *106* (18), 187201.
- 13
14 (26) Wäckerlin, C.; Chylarecka, D.; Kleibert, A.; Müller, K.; Iacovita, C.; Nolting, F.; Jung, T. A.; Ballav, N. Controlling Spins in Adsorbed Molecules by a Chemical Switch. *Nat. Commun.* **2010**, *1* (1), 61.
- 15
16 (27) Li, R.; Li, N.; Wang, H.; Weismann, A.; Zhang, Y.; Hou, S.; Wu, K.; Wang, Y. Tuning the Spin-Related Transport Properties of FePc on Au(111) through Single-Molecule Chemistry. *Chem. Commun.* **2018**, *54* (66), 9135–9138.
- 17
18 (28) Li, J.; Friedrich, N.; Merino, N.; de Oteyza, D. G.; Peña, D.; Jacob, D.; Pascual, J. I. Electrically Addressing the Spin of a Magnetic Porphyrin through Covalently Connected Graphene Electrodes. *Nano Lett.* **2019**, *19* (5), 3288–3294.
- 19
20 (29) Li, J.; Merino-Díez, N.; Carbonell-Sanromà, E.; Vilas-Varela, M.; de Oteyza, D. G.; Peña, D.; Corso, M.; Pascual, J. I. Survival of Spin State in Magnetic Porphyrins Contacted by Graphene Nanoribbons. *Sci. Adv.* **2018**, *4* (2) eaaq0582.
- 21
22 (30) Su, X.; Xue, Z.; Li, G.; Yu, P. Edge State Engineering of Graphene Nanoribbons. *Nano Lett.* **2018**, *18* (9), 5744–5751.
- 23
24 (31) Mateo, L. M.; Sun, Q.; Liu, S.-X.; Bergkamp, J. J.; Eimre, K.; Pignedoli, C. A.; Ruffieux, P.; Decurtins, S.; Bottari, G.; Fasel, R.; Torres, T. On-Surface Synthesis and Characterization of Triply Fused Porphyrin–Graphene Nanoribbon Hybrids. *Angew. Chem. Int. Ed.* **2020**, *59* (3), 1334–1339.
- 25
26 (32) He, Y.; Garnica, M.; Bischoff, F.; Ducke, J.; Bocquet, M.-L.; Batzill, M.; Auwärter, W.; Barth, J. V. Fusing Tetrapyrroles to Graphene Edges by Surface-Assisted Covalent Coupling. *Nat. Chem.* **2017**, *9* (1), 33–38.
- 27
28 (33) Bischoff, F.; He, Y.; Riss, A.; Seufert, K.; Auwärter, W.; Barth, J. V. Exploration of Interfacial Porphine Coupling Schemes and Hybrid Systems by Bond-Resolved Scanning Probe Microscopy. *Angew. Chem. Int. Ed.* **2018**, *57* (49), 16030–16035.
- 29
30 (34) Lieb, E. H. Two Theorems on the Hubbard Model. *Phys. Rev. Lett.* **1989**, *62* (10), 1201–1204.
- 31
32 (35) Yazyev, O. V.; Helm, L. Defect-Induced Magnetism in Graphene. *Phys. Rev. B* **2007**, *75* (12), 125408.
- 33
34 (36) Wang, W. L.; Yazyev, O. V.; Meng, S.; Kaxiras, E. Topological Frustration in Graphene Nanoflakes: Magnetic Order and Spin Logic Devices. *Phys. Rev. Lett.* **2009**, *102* (15), 157201.
- 35
36 (37) Yazyev, O. V. Emergence of Magnetism in Graphene Materials and Nanostructures. *Rep. Prog. Phys.* **2010**, *73* (5), 056501.
- 37
38 (38) Ortiz, R.; Lado, J. L.; Melle-Franco, M.; Fernández-Rossier, J. Engineering Spin Exchange in Nonbipartite Graphene Zigzag Edges. *Phys. Rev. B* **2016**, *94* (9), 094414.
- 39
40 (39) Ruffieux, P.; Wang, S.; Yang, B.; Sánchez-Sánchez, C.; Liu, J.; Dienel, T.; Talirz, L.; Shinde, P.; Pignedoli, C. A.; Passerone, D.; Dumlaff, T.; Feng, X.; Müllen, K.; Fasel, R. On-Surface Synthesis of Graphene Nanoribbons with Zigzag Edge Topology. *Nature* **2016**, *531*, 489.
- 41
42 (40) Gonzalez-Herrero, H.; Gomez-Rodriguez, J. M.; Mallet, P.; Moaied, M.; Palacios, J. J.; Salgado, C.; Ugeda, M. M.; Veuillen, J.-Y.; Yndurain, F.; Brihuega, I. Atomic-Scale Control of Graphene Magnetism by Using Hydrogen Atoms. *Science* **2016**, *352* (6284), 437–441.
- 43
44 (41) Pavliček, N.; Mistry, A.; Majzik, Z.; Moll, N.; Meyer, G.; Fox, D. J.; Gross, L. Synthesis and Characterization of Triangulene. *Nat. Nanotechnol.* **2017**, *31*.
- 45
46 (42) Mishra, S.; Lohr, T. G.; Pignedoli, C. A.; Liu, J.; Berger, R.; Urgel, J. I.; Müllen, K.; Feng, X.; Ruffieux, P.; Fasel, R. Tailoring Bond Topologies in Open-Shell Graphene Nanostructures. *ACS Nano* **2018**, *12* (12), 11917–11927.
- 47
48 (43) Mishra, S.; Beyer, D.; Eimre, K.; Liu, J.; Berger, R.; Gröning, O.; Pignedoli, C. A.; Müllen, K.; Fasel, R.; Feng, X.; Ruffieux, P. Synthesis and Characterization of π -Extended Triangulene. *J. Am. Chem. Soc.* **2019**, *141* (27), 10621–10625.
- 49
50
51
52
53
54
55
56
57
58
59
60

- 1
2
3 (44) Ortiz, R.; Boto, R. A.; García-Martínez, N.; Sancho-García, J. C.; Melle-Franco, M.; Fernández-Rossier, J. Exchange Rules for Diradical π -Conjugated Hydrocarbons. *Nano Lett.* **2019**, *19* (9), 5991–5997.
- 4 (45) Li, J.; Sanz, S.; Corso, M.; Choi, D. J.; Peña, D.; Frederiksen, T.; Pascual, J. I. Single Spin Localization and Manipulation in Graphene Open-Shell Nanostructures. *Nat. Commun.* **2019**, *10* (1), 200.
- 5 (46) Mishra, S.; Beyer, D.; Berger, R.; Liu, J.; Gröning, O.; Urgel, J. I.; Müllen, K.; Ruffieux, P.; Feng, X.; Fasel, R. Topological Defect-Induced Magnetism in a Nanographene. *J. Am. Chem. Soc.* **2020**, *142* (3), 1147–1152.
- 6 (47) Mishra, S.; Beyer, D.; Eimre, K.; Kezilebieke, S.; Berger, R.; Gröning, O.; Pignedoli, C. A.; Müllen, K.; Liljeroth, P.; Ruffieux, P.; Feng, X.; Fasel, R. Topological Frustration Induces Unconventional Magnetism in a Nanographene. *Nat. Nanotechnol.* **2020**, *15* (1), 22–28.
- 7 (48) Mishra, S.; Beyer, D.; Eimre, K.; Ortiz, R.; Fernández-Rossier, J.; Ber, R. Collective All-Carbon Magnetism in Triangulene Dimers. *Angew. Chem. Int. Ed.* **2020** *59* (29), 12041–12047.
- 8 (49) Zheng, Y.; Li, C.; Zhao, Y.; Beyer, D.; Wang, G.; Xu, C.; Yue, X.; Chen, Y.; Guan, D.-D.; Li, Y.-Y.; Zheng, H.; Liu, C.; Luo, W.; Feng, X.; Wang, S.; Jia, J. Engineering of Magnetic Coupling in Nanographene. *Phys. Rev. Lett.* **2020**, *124* (14), 147206.
- 9 (50) Yuan, B.; Li, C.; Zhao, Y.; Gröning, O.; Zhou, X.; Zhang, P.; Guan, D.; Li, Y.; Zheng, H.; Liu, C.; Mai, Y.; Liu, P.; Ji, W.; Jia, J.; Wang, S. Resolving Quinoid Structure in Poly(Para-Phenylene) Chains. *J. Am. Chem. Soc.* **2020**, *142* (22), 10034–10041.
- 10 (51) Su, J.; Telychko, M.; Hu, P.; Macam, G.; Mutombo, P.; Zhang, H.; Bao, Y.; Cheng, F.; Huang, Z.-Q.; Qiu, Z.; Tan, S. J. R.; Lin, H.; Jelínek, P.; Chuang, F.-C.; Wu, J.; Lu, J. Atomically Precise Bottom-up Synthesis of π -Extended [5]Triangulene. *Sci. Adv.* **2019**, *5* (7), 7717.
- 11 (52) Sánchez-Grande, A.; Urgel, J. I.; Cahlik, A.; Santos, J.; Edalatmanesh, S.; Rodríguez-Sánchez, E.; Lauwaet, K.; Mutombo, P.; Nachtigallová, D.; Nieman, R.; Lischka, H.; de la Torre, B.; Miranda, R.; Gröning, O.; Martín, N.; Jelínek, P.; Écija, D. Diradical Organic One-dimensional Polymers Synthesized on a Metallic Surface. *Angew. Chem. Int. Ed.* **2020**, ange.202006276.
- 12 (53) Lash, T. D. Origin of Aromatic Character in Porphyrinoid Systems. *J. Porphyr. Phthalocyanines* **2011**, *15* (11n12), 1093–1115..
- 13 (54) Zugermeier, M.; Herritsch, J.; Luy, J.-N.; Chen, M.; Klein, B. P.; Niefind, F.; Schweyen, P.; Bröring, M.; Schmid, M.; Tonner, R.; Gottfried, J. M. On-Surface Formation of a Transient Corrole Radical and Aromaticity-Driven Interfacial Electron Transfer. *J. Phys. Chem. C* **2020**, *124* (25), 13825–13836.
- 14 (55) Zeng, W.; Lee, S.; Son, M.; Ishida, M.; Furukawa, K.; Hu, P.; Sun, Z.; Kim, D.; Wu, J. Phenalenyl-Fused Porphyrins with Different Ground States. *Chem. Sci.* **2015**, *6* (4), 2427–2433.
- 15 (56) Shimizu, D.; Osuka, A. Porphyrinoids as a Platform of Stable Radicals. *Chem. Sci.* **2018**, *9* (6), 1408–1423.
- 16 (57) Beyer, D.; Wang, S.; Pignedoli, C. A.; Melidonie, J.; Yuan, B.; Li, C.; Wilhelm, J.; Ruffieux, P.; Berger, R.; Müllen, K.; Fasel, R.; Feng, X. Graphene Nanoribbons Derived from Zigzag Edge-Encased Poly(Para-2,9-Dibenzo[Bc,Kl]Corononylene) Polymer Chains. *J. Am. Chem. Soc.* **2019**, *141* (7), 2843–2846.
- 17 (58) Sun, Z.; Wu, J. Open-Shell Polycyclic Aromatic Hydrocarbons. *J. Mater. Chem.* **2012**, *22* (10), 4151–4160.
- 18 (59) Clar, E. *Polycyclic Hydrocarbons*; Springer-Verlag Berlin Heidelberg, 1964.
- 19 (60) van der Lit, J.; Boneschanscher, M. P.; Vanmaekelbergh, D.; Ijäs, M.; Uppstu, A.; Ervasti, M.; Harju, A.; Liljeroth, P.; Swart, I. Suppression of Electron–Vibron Coupling in Graphene Nanoribbons Contacted via a Single Atom. *Nat. Commun.* **2013**, *4* (1), 2023.
- 20 (61) Wang, S.; Talirz, L.; Pignedoli, C. A.; Feng, X.; Müllen, K.; Fasel, R.; Ruffieux, P. Giant Edge State Splitting at Atomically Precise Graphene Zigzag Edges. *Nat. Commun.* **2016**, *7*, 11507.
- 21 (62) Kondo, J. Resistance Minimum in Dilute Magnetic Alloys. *Prog. Theor. Phys.* **1964**, *32* (1), 37–49.
- 22 (63) Shinde, P. P.; Gröning, O.; Wang, S.; Ruffieux, P.; Pignedoli, C. A.; Fasel, R.; Passerone, D. Stability of Edge Magnetism in Functionalized Zigzag Graphene Nanoribbons. *Carbon* **2017**, *124*, 123–132.
- 23
24
25
26
27
28
29
30
31
32
33
34
35
36
37
38
39
40
41
42
43
44
45
46
47
48
49
50
51
52
53
54
55
56
57
58
59
60

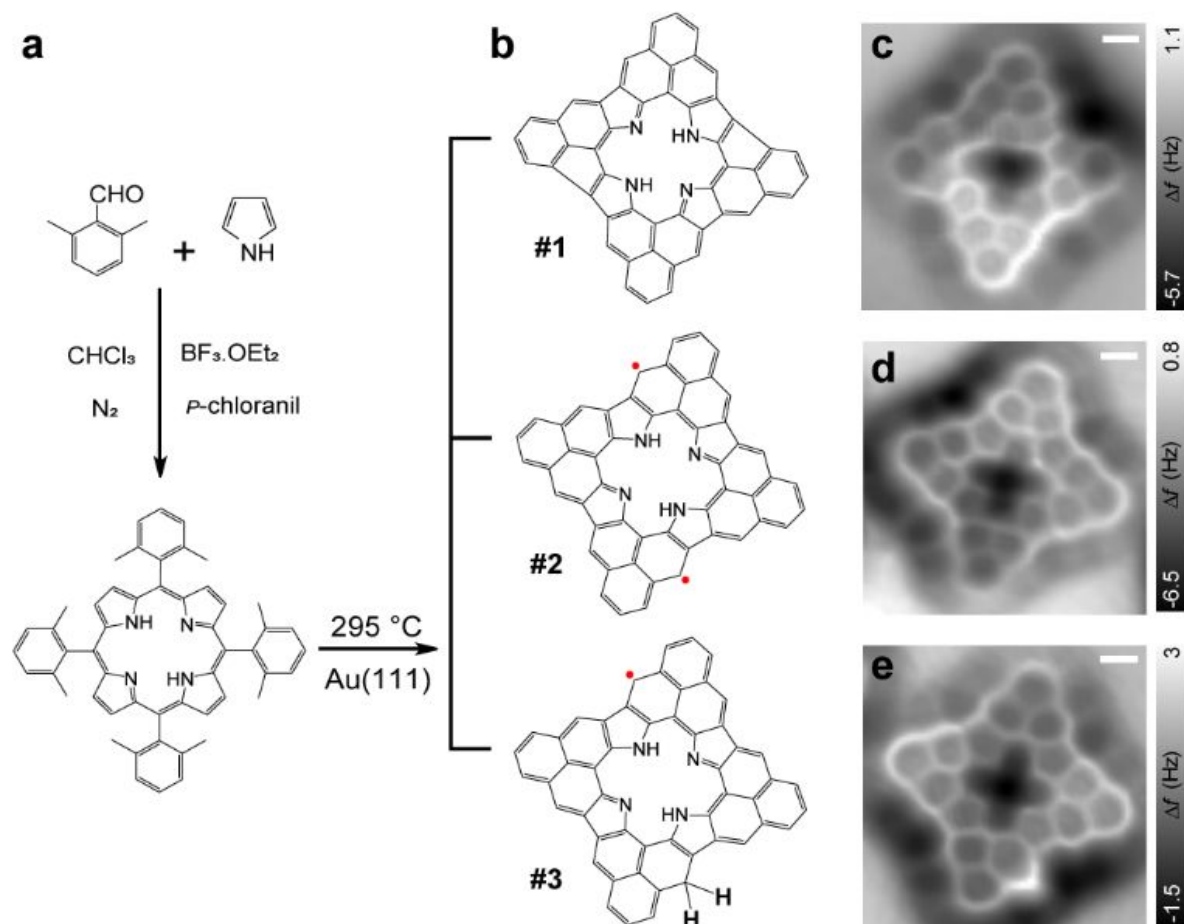


Figure 1. Synthesis of porphyrins with different π -electron topologies. (a), In-solution synthesis of molecular precursor 5,10,15,20-tetrakis(2,6-dimethylphenyl) porphyrin. (b), Chemical structures of three On-surface synthesized porphyrins with red dots indicating the unpaired π -electrons. (c-e), Nc-AFM frequency shift images (Resonant frequency: 26 KHz, Oscillation amplitude: 80 pm, Scale bars: 0.4 nm) of the porphyrins in (b).

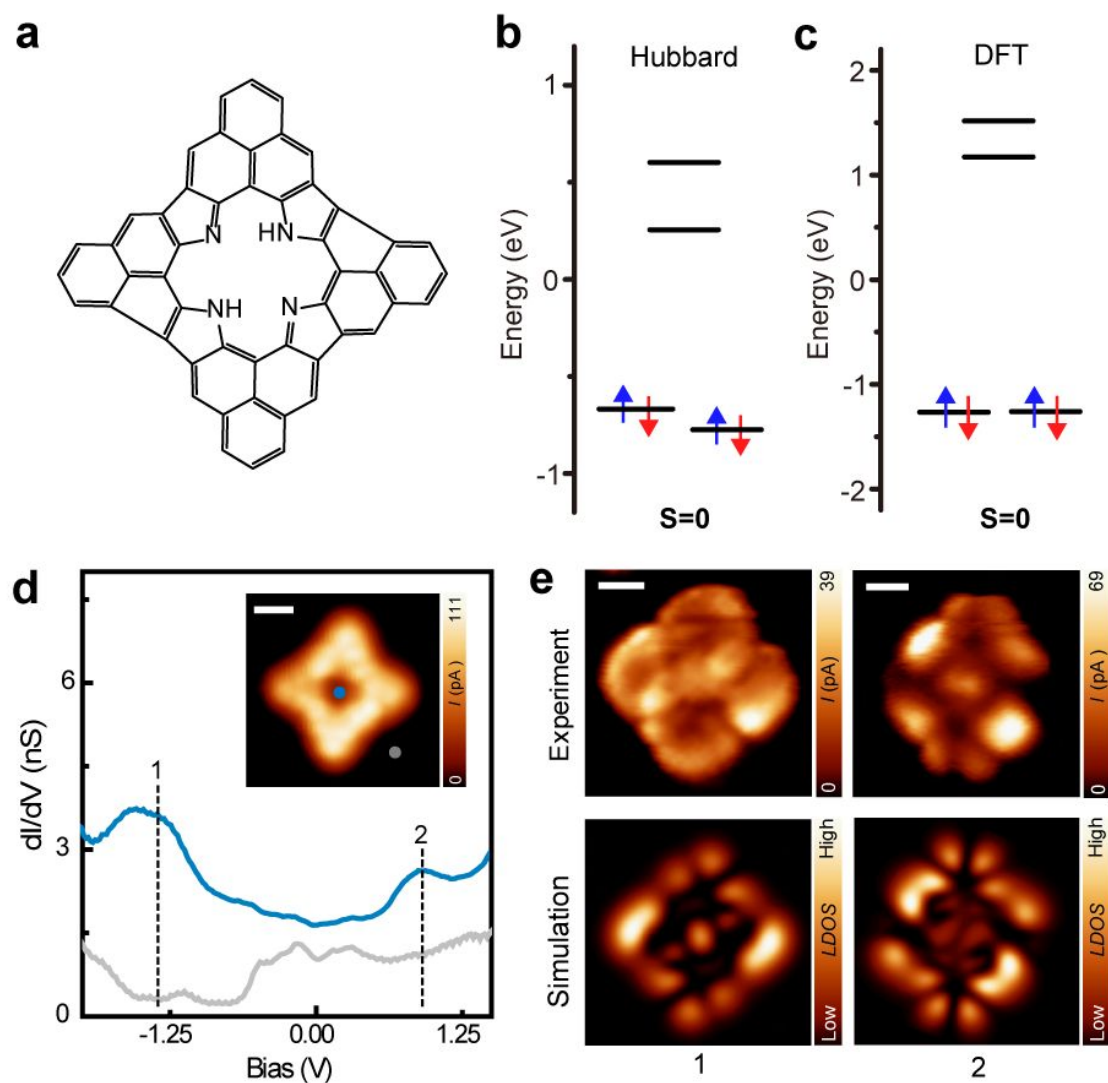


Figure 2. Electronic structure of a closed-shell porphyrin with two embedded pentagon rings. (a), Chemical structure of the product #1. (b-c), Mean-field Hubbard model and spin-polarized density functional theory calculated energy spectrum of the porphyrin in (a). (d), dI/dV spectra taken at the two locations marked on the inset constant-height current image (Bias: 10 mV; scale bar: 0.25 nm). The resonance below fermi level is assigned to the superposition of HOMO-1 and HOMO, and the resonance above fermi level to LUMO. (e), Up: spatial resolved local density of states maps taken at the biases marked by dashed lines in (d); Down: DFT simulated density of states maps. Scale bars: 0.5 nm.

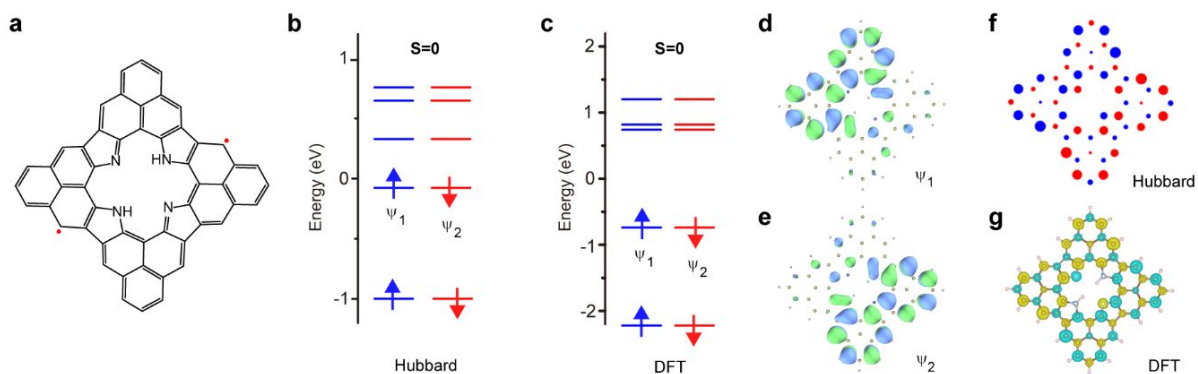


Figure 3. Spin polarized singlet ground state in the Product #2. (a), Chemical structure of the Product #2 with two unpaired π electrons as marked by red dots. (b-c), Mean-field Hubbard model and spin-polarized density functional theory calculated energy spectrum of the porphyrin in (a). (d-e), DFT calculated frontier orbitals of the two singly occupied states as marked in (b) and (c). (f-g), Mean-field Hubbard model and spin-polarized density functional theory calculated spin density distributions. Red/green: spin up, blue/yellow: spin down.

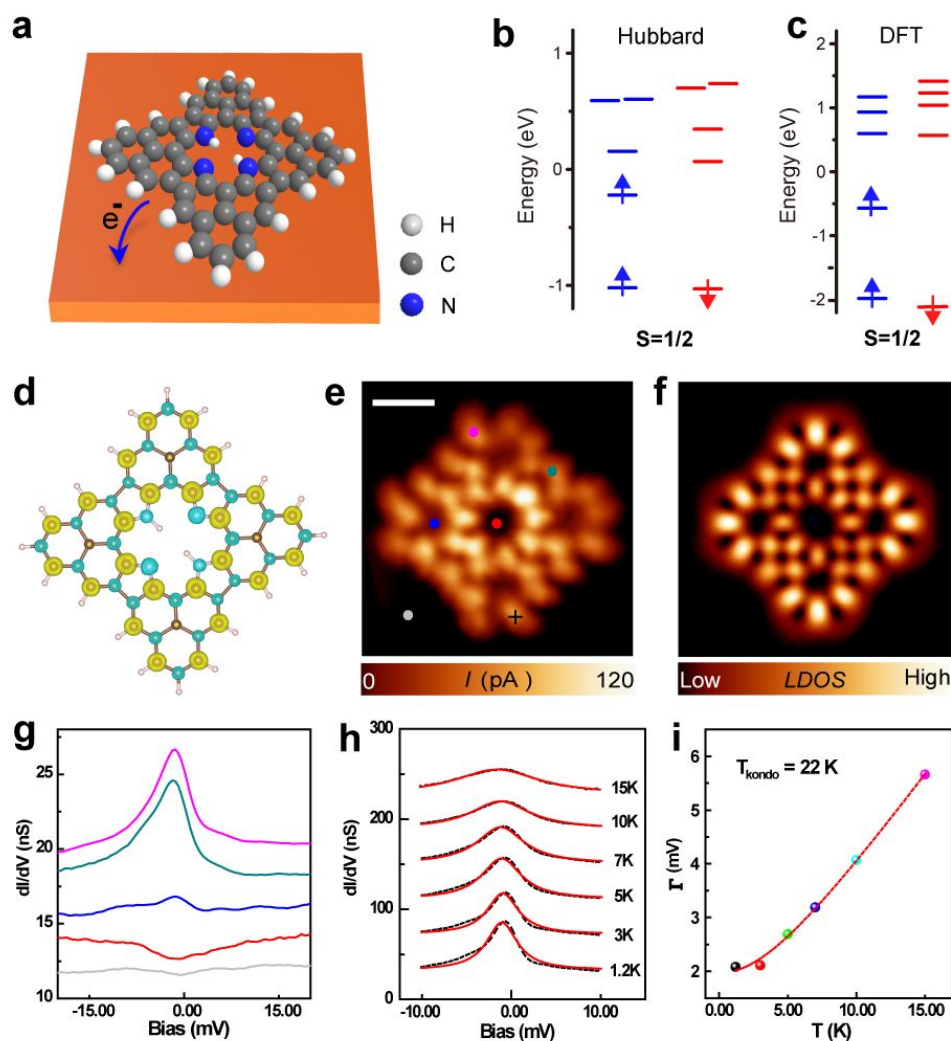


Figure 4. Electronic structure of the positively charged Product #2. (a), Illustrative showing charge transfer from the Product #2 to underneath Au(111), thus making it positively charged. (b-c), Mean-field Hubbard model and spin-polarized density functional theory calculated energy spectrum of the charged Product #2. (d), Spin-polarized DFT calculated spin density distributions. Green: spin up, Yellow: spin down. (e-f), Constant-height current image (Bias voltage: 1 mV, Scale bars: 0.5 nm), and DFT simulated SOMO LDOS map of the charged Product #2. (g), dI/dV spectra taken on the locations marked in (e). (h), Temperature dependent dI/dV spectra showing the broadening of Kondo resonance peak as increase the temperature. The dashed lines are fitted curves using a Frota function. The spectra are taken at the position marked by a cross in (e). (i), The full-width at half maximum of Kondo resonance peak as a function of temperature. The solid red line is fitted curve giving a Kondo temperature of 22K.

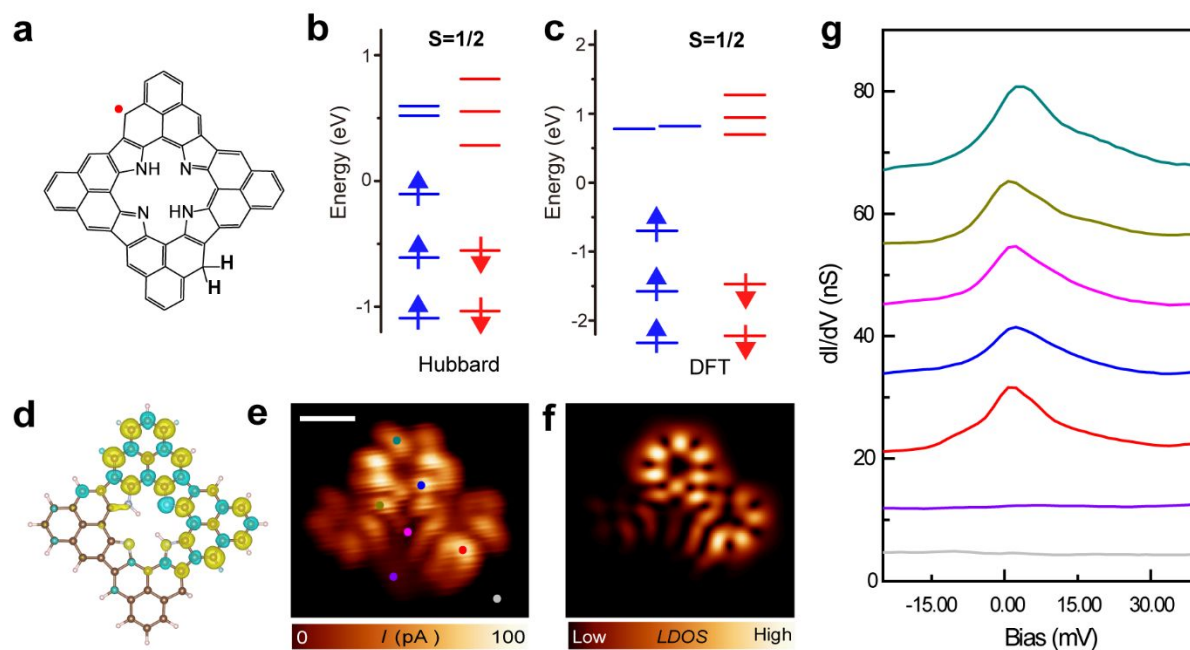


Figure 5. Electronic structure of the Product #3. (a), Chemical structure of the Product #3 with one unpaired π electron as marked by a red dot. (b-c), Mean-field Hubbard model and spin-polarized density functional theory calculated energy spectrum of the Product #3. (d), Spin-polarized density functional theory calculated spin density distributions. Green: spin up, Yellow: spin down. (e-f), Constant-height current image (Bias voltage: 1 mV, Scale bars: 0.5 nm), and DFT simulated SOMO LDOS map of the Product #3. (g), dI/dV spectra taken at the locations marked in (e).

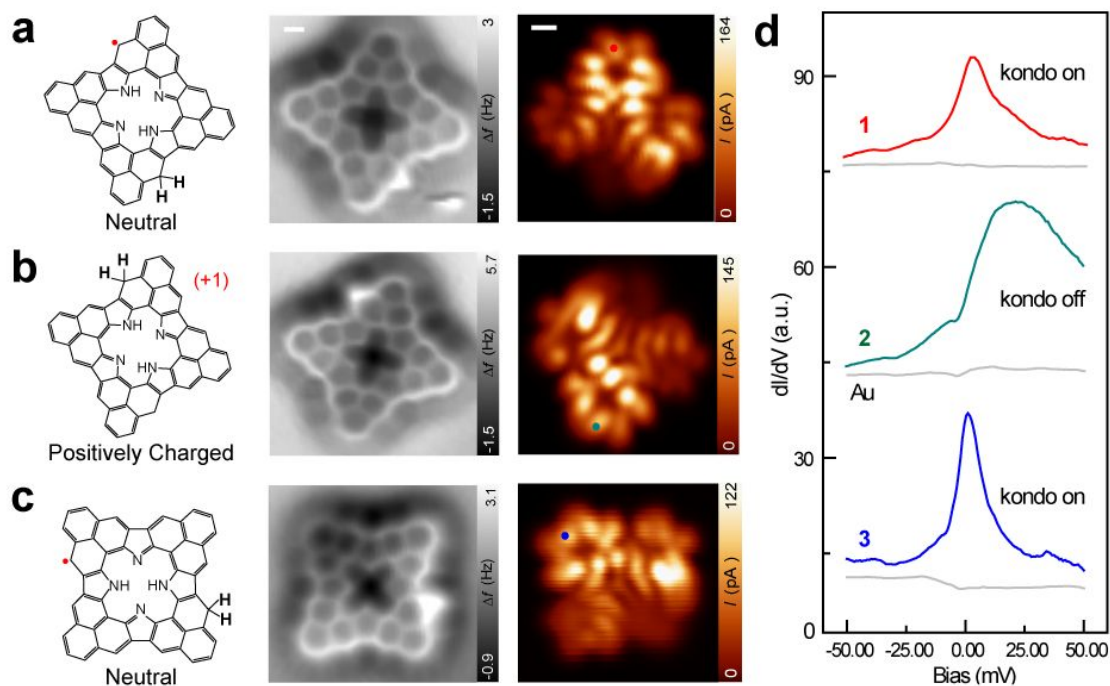
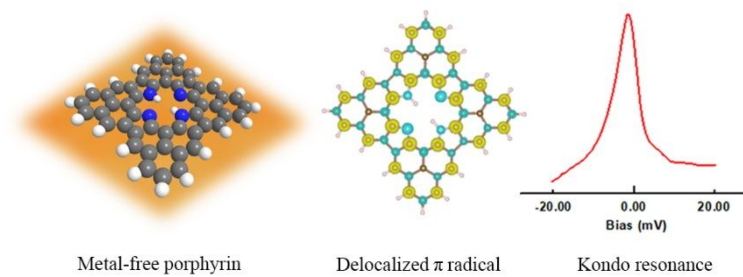


Figure 6. Switching magnetic state by STM manipulation. (a-c), From left to right: Chemical structure, nc-AFM image (Resonant frequency: 26 KHz, Oscillation amplitude: 80 pm, Scale bars: 0.2 nm), Constant-height current image (Bias voltage: 1 mV, Scale bars: 0.25 nm) of the Product #3 after two manipulation steps. (d), dI/dV spectra taken at the marked positions in (a-c).

TOC Figure



Metal-free porphyrin

Delocalized π radical

Kondo resonance